Title

Evaluation of thermo-mechanical and thermal behavior of full-scale energy foundations

Authors

Murphy, Kyle D
McCartney, John S
Henry, Karen S

1 **Evaluation of Thermo-Mechanical and Thermal Behavior of Full-Scale Energy**
2 **Foundations**

3 Kyle D. Murphy[1], John S. McCartney[2], and Karen S. Henry[3]

4 [1]Graduate Research Assistant, University of Colorado Boulder, Dept. of Civil, Env. and Arch.
5 Engineering, UCB 428, Boulder, CO 80309, kyle.murphy@colorado.edu

6 [2]Associate Professor and Lyall Faculty Fellow, University of Colorado Boulder, Dept. of Civil,
7 Env. and Arch. Engineering, UCB 428, Boulder, CO 80309, john.mccartney@colorado.edu

8 [3]Associate Professor, United States Air Force Academy, Department of Civil Engineering,
9 USAF Academy, CO 80840-6232, karen.henry@usafa.edu

10 **Abstract**

11 Eight full-scale energy foundations were constructed for a new building at the U.S. Air Force
12 Academy (USAFA). The foundations are being used to demonstrate this technology to the
13 United States Department of Defense, and have several experimental features in order to study of
14 their thermal-mechanical behavior. Three of the foundations are instrumented with strain gages
15 and thermistors, and their thermo-mechanical response during a heating and cooling test were
16 evaluated. For a temperature increase of 18°C, the maximum thermal axial stress ranged from
17 4.0 to 5.1 MPa, which is approximately 25% of the compressive strength of concrete (estimated
18 at 21 MPa) and the maximum upward displacement ranged from 1.4 to 1.7 mm, which should
19 not cause angular distortions sufficient enough to cause structural or aesthetic damage of the
20 building. The end restraint provided by the building was observed to change depending on the
21 location of the foundation. The heat flux per meter was measured by evaluating the temperatures
22 and flow rates of a heat exchanger fluid entering and exiting the foundations. The heat flux
23 values were consistent with those in the literature, and the foundation with the 3 continuous heat
24 exchanger loops was found to have the greatest heat flux per meter. The transient thermal
25 conductivity of the subsurface measured using the temperatures of the subsurface surrounding
26 the foundation ranged from 2.0 to 2.3 W/mK, which is consistent with results from thermal
27 response tests on energy foundations reported in the literature.

28 <u>Keywords</u>: Geothermal Heat Exchange, Deep Foundations, Thermo-Mechanical Behavior;
29 Thermal Response Test

30

31

32

33

1 Introduction

Heating and cooling of buildings comprises nearly 50% of the total building energy usage in the United States (Energy Information Administration 2008). Ground-source heat exchange (GSHE) systems are an approach to reduce the energy demand of heating and cooling systems compared to conventional air-source heat pump systems. The most common GSHE system involves the use of a closed loop heat exchanger to transfer heat between the subsurface soil or rock and an overlying structure, taking advantage of the relatively constant natural ground temperature below the depth of seasonal variation (Brandl 2006). The subsurface below a depth of 4 m generally has a relatively constant temperature approximately equal to the mean annual air temperature at a given location, and thus permits the efficiency of a ground-source heat exchange system to be higher than that of an air-source heat exchange system (Kavanaugh et al. 1997).

Although conventional ground-source heat exchange (GSHE) systems have been used for many years, the additional cost of drilling deep boreholes for the sole purpose of exchanging heat with the ground has rendered this technology cost-prohibitive in some situations (Hughes 2008). Energy foundations are a feasible approach to enhance implementation of GSHE systems by reducing installation costs through taking advantage of initial construction activities (Brandl 2006; Adam and Markiewicz 2009). In this study, energy foundations refer to drilled shaft foundations constructed with a set of closed-loop heat exchangers attached to the inside of the reinforcement cage so that they can serve the dual purposes of providing structural support and providing access to ground thermal energy. While energy foundations are gaining popularity throughout the world, further research is required to fully understand their performance in terms of thermal response and thermo-mechanical behavior in different soil profiles. This paper focuses on the characterization of a series of eight energy foundations installed in an unsaturated sandstone deposit.

2 Background

2.1 Thermo-mechanical Behavior

As a deep foundation is loaded mechanically, the axial stress is expected to be highest at the head and decrease with depth as side shear resistance is mobilized at the soil-foundation interface. The axial stress will decrease to zero if the side shear resistance is sufficient to support the building load; if not, it will decrease to a non-zero value and there will be end bearing resistance in the material underlying the toe of the foundation. As an energy foundation is heated or cooled, the reinforced concrete will tend to expand or contract axially about a point referred to as the "null point" (Knellwolf et al. 2011). The null point is the point of zero axial displacement during heating or cooling, and its location depends on the stiffness of the end boundaries imposed by the overlying superstructure and the material beneath the toe, as well as the distribution of mobilized side shear resistance (Bourne-Webb et al. 2009; Amatya et al. 2012). It

71 is also likely that radial expansion of the foundation will occur as the foundation is heated
72 (Laloui et al. 2006), which may result in a net increase in ultimate side shear resistance
73 (McCartney and Rosenberg 2011; Ouyang et al. 2011).

74   The upper limit on the thermal axial strain ε_T in an energy foundation is the free expansion
75 (i.e., unrestrained) thermal axial strain $\varepsilon_{T,free}$, defined as follows:

$$\varepsilon_{T,free} = \alpha_c \Delta T \qquad\qquad (1)$$

76 where α_c is the coefficient of linear thermal expansion of reinforced concrete and ΔT is the
77 change in temperature. For geotechnical engineering purposes, the thermal axial strain is defined
78 as positive during compression. Accordingly, α_c is defined as negative because structural
79 elements expand during heating (i.e., positive ΔT). For the case that an energy foundation is
80 restrained from moving such that the actual thermal axial strain ε_T is less than that predicted by
81 Equation 1, the thermal axial stresses σ_T can be calculated as follows:

$$\sigma_T = E(\varepsilon_T - \alpha_c \Delta T) \qquad\qquad (2)$$

82 where E is the Young's modulus of reinforced concrete. For energy foundations, soil-structure
83 interaction mechanisms will restrict the movement of the foundation during heating. The side
84 shear resistance, end bearing, and building restraint will influence the distribution in thermally
85 induced stresses and strains (Mimouni and Laloui 2013). Soil-structure interaction mechanisms
86 of energy foundations have been studied in centrifuge-scale tests for simplified soil profiles
87 (McCartney and Rosenberg 2011; Stewart and McCartney 2014). However, evaluation of full-
88 scale foundations imposes a set of real boundary conditions and soil strata. Several full-scale
89 energy foundations have been evaluated to study the thermo-mechanical stresses and strains
90 during mechanical loading, heating, and cooling (Laloui et al. 2006; Bourne-Webb et al. 2009;
91 Amatya et al. 2012; McCartney and Murphy 2012) (Table 1). The thermal axial stress ranges
92 from -1 to 5MPa and the thermal axial displacement of the foundation head ranges from -4.2 mm
93 upward to +4.0 downward. The axial stresses are well within the compressive strength of
94 reinforced concrete, and the axial displacements of the foundation would not lead to significant
95 angular distortions to cause architectural damage for most buildings.

96 **2.2 Thermal Behavior**

97   The thermal behavior of energy foundations depends on many factors including the thermal
98 properties of individual materials in the GSHE, site stratigraphy, groundwater and its flow, heat
99 exchanger configuration within foundation and dimensions of the energy foundation, and thermal
100 demands of the building (Brandl 2006). To optimize the design of GSHE, the system thermal
101 conductivity, specific heat capacity, borehole resistance, and heat exchange rate must be
102 evaluated accurately (Sanner 2001). For the purposes of this study, the primary mode of heat
103 transport in the soil surrounding energy foundations is assumed to be by conduction. There is
104 little to no groundwater present in the soil profile of the foundation installations, hence

105 groundwater flow (and convective heat transfer) is considered to be negligible. The heat flux
106 from a cylindrical source (i.e., an energy foundation) is given by:

$$Q = -2\pi Rl\lambda \frac{dT}{dr}$$ **(3)**

107 where Q is the heat flux in Watts being supplied to the energy foundation, R is the radius of the
108 energy foundation, l is the length of the energy foundation, λ is the thermal conductivity of the
109 medium in contact with the cylindrical source, and dT/dr is the temperature gradient in the radial
110 direction. Convection is the main heat flow process in the fluid itself as the fluid flow rate is
111 sufficient to lead to a turbulent flow pattern, while conduction is dominant through the heat
112 exchanger pipe, concrete, and into the ground. As it is difficult to measure the thermal properties
113 of the individual soil layers and materials in energy foundations, they are typically characterized
114 using a system value.

115   Thermal response tests (TRT) are the most common method of determining thermal
116 properties of the subsurface and energy foundation system (Brandl 2006). Thermal response
117 testing of geothermal borehole heat exchangers has been in use for several years (Sanner et al.
118 2005), and involves circulating a fluid through a heat exchanger while supplying a constant
119 amount of power to the fluid. During a TRT the temperatures of the fluid entering and exiting the
120 foundation are monitored over a period of several days. The measured values of the fluid supply
121 and return temperatures and the mass flow rate through each foundation can be used to calculate
122 the input heat flux, as follows:

$$Q = \Delta T \dot{V} \rho_{fluid} C_{fluid}$$ **(4)**

123 where ΔT is the difference between the supply and return fluid temperatures in K (T_{supply} and
124 T_{return}, respectively), $\dot{V}$ is the fluid flow rate in m^3/s, ρ_{fluid} is the mass density of the fluid kg/m^3,
125 and C_{fluid} is the specific heat capacity of the fluid in J/(kgK). The heat flux density can be
126 calculated by dividing Equation (4) by the cross-sectional area of the heat exchanger tubing.

127   Several studies have used the simple analytical solutions to investigate the thermal behavior
128 of full-scale energy foundations in different soil types with various heat exchanger loop
129 configurations and foundation geometries (Hamada et al. 2007; Ooka 2007; Gao 2008; Lennon et
130 al. 2009; Brettmann and Amis 2011). The results of these studies are summarized in Table 2. The
131 system thermal conductivity values reported in these studies ranges from 2.4 to 6.0 W/mK,
132 which is much higher than the thermal conductivity of most geological and structural materials,
133 suggesting that the thermal conductivity values may incorporate the effects of the heat capacity
134 of the concrete and may not represent steady-state conditions (Loveridge and Powrie 2012). In
135 these studies, the TRT was performed at the head of the foundation before the building has been
136 constructed. However, there has not been a thorough evaluation of TRT results on foundations
137 after construction and plumbing is complete. The fact that the tubing used to connect the energy
138 foundation to the heat pump is often not insulated for practical construction purposes means that

139 the heat exchange response of the energy foundation system may be affected by ambient surface
140 fluctuations.

3 Project Description

3.1 Building Description

143   A one-story, shower-shave building was constructed at the Field Engineering and Readiness
144 Laboratory (FERL) of the US Air Force Academy (USAFA) beginning March, 2012. The
145 building provides restrooms, showers, and laundry facilities for 100 people. The building will
146 also be used to evaluate the performance of energy efficient technologies to aid in the
147 development of "net zero" energy consuming structures for the U.S. Department of Defense
148 (DoD). These technologies include energy foundations, a radiant in-floor heating system, solar
149 photovoltaic panels, and a solar water heating system. Each component will be continuously
150 monitored to evaluate the energy usage or output of each technology. In addition to the ground-
151 source heat pump coupled with the energy foundations, the building contains a natural gas boiler
152 heating system. Having both conventional and ground-source HVAC systems permits
153 comparison of their energy efficiencies under similar environmental conditions.

3.2 Subsurface Conditions

155   A site investigation was performed in September 2011 by Hernandez (2011), which consisted
156 of two 102 mm-diameter borings located within the building footprint, extending 12 and 7 m
157 below the ground surface. At selected intervals, disturbed samples were obtained by driving
158 split-spoon with a 622.75 N hammer falling 762 mm. Penetration resistance measurements were
159 made during driving. Exploration results from both boreholes were similar and showed three
160 prominent strata, and relevant data is shown in Table 3. The thermal conductivity values were
161 measured on the split-spoon samples of soil using a thermal needle, and provide a preliminary
162 estimate of the thermal conductivity of the subsurface strata. The top layer is approximately 1 m
163 thick and consists of sandy fill. Beneath the fill is a very dense 1 m-thick sandy gravelly layer.
164 The bedrock is Dawson-Arkose (sandstone) extending to the maximum depth explored. No
165 groundwater was encountered during the site investigation or foundation installation, so it is
166 assumed to be at a depth greater than 16 m.

3.3 Energy Foundation Descriptions

168   Eight drilled shafts, each 15.2 m deep by 0.61 m diameter, provide the foundation support for
169 the structure, as shown in Figure 1(a). The one-story building could have been constructed with a
170 shallow foundation, so the main purpose of incorporating the deep drilled shafts into the building
171 was to evaluate the thermo-mechanical response of the energy foundations for this research
172 project. Each foundation contains a 0.46-m-diameter steel reinforcing cage that extends the full
173 length of the shaft. The reinforcing cages are composed of six #7 longitudinal bars with #5 radial
174 hoops spaced at 0.3 m on center throughout the length of the cage. The top of the shafts are

175 spliced into a 0.91 m-deep by 0.61 m-wide grade beam that extends around the perimiter of the
176 building. Each foundation contains a heat exchanger loop consisting of 19 mm-diameter HDPE
177 tubing. At the top of each foundation, (1 meter below grade), the heat exchanger loop is
178 connected with tubing which is routed through the grade beam [Fig. 1(b)] into a manifold within
179 the mechanical room of the building [Fig. 1(c)].

180 The heat exchange tubing was attached to the inside of the reinforcing cages such that the
181 inlet and outlet tubes were seperated diametrically by at least 90°, which minimizes thermal short
182 circuiting from the inlet to outlet tubes. The reinforcing cages were lifted with a 3-point pick to
183 minimize bending, and the cages were lowered into the hole with a crane and were suspended on
184 wooden beams to ensure that the top of the cage was at the base of the grade beam. A concrete
185 pump truck was used to place high-slump concrete with a compressive strength (f'$_c$) of 21 MPa
186 in the holes following placement of the reinforcing cages. A tremie pipe was used to avoid
187 excessive segragation of the concrete during free-fall. The use of the tremie also minimized the
188 risk of damage to the heat exchanger loops and embedded instrumentation.

189 Each shaft has either one, two, or three heat exhanger loops configured in different ways,
190 (Figure 2). Foundations 1 through 4 have identical heat exchanger configurations, with two
191 continuous heat exchanger loops attached to the inside of the steel reinforcement cage.
192 Foundation 5 has three individual loops; each having a supply and return line running to the
193 mechanical room; this permits any combination of the loops to be operational in order to
194 evaluate the efficiency of multiple loops in a single foundation. Foundation 6 has three
195 continuous heat exchanger loops with only one supply and return line extending to the
196 manifolds. Foundation 7 contains one loop connected to the interior of the reinforcing cage.
197 Foundation 8 has a single loop in the center of the foundation to simulate a retrofit where a heat
198 exchanger would be inserted into a corehole bored into an existing foundation. This was
199 constructed with a 100 mm-diameter plastic sleeve in the center of the foundation. After curing,
200 a single heat exchanger loop was inserted into the plastic sleeve and the hole was grouted with
201 sand bentonite grout.

202 **3.4 Instrumentation**

203 Instrumentation was incorporated into three of the eight energy foundations to capture the
204 distribution of axial strain and temperature with depth. Foundations 1 and 3 contain six Geokon
205 Model 4200 vibrating wire strain gauges (VWSGs), while Foundation 4 contains twelve, at the
206 depths shown in Figure 4. Foundation 4 has twice the number of gauges to capture detailed strain
207 and temperature distribution. At three locations within Foundation 4, gauges were located at the
208 same depth on opposite sides of the reinforcing gage to gain redundancy in temperature and
209 strain readings and to capture any differential strain measurements across the width of the shaft.
210 All of the gauges were oriented vertically and attached to brackets welded to longitudinal steel
211 reinforcing bars. The sensor cables were routed to the mechanical room where they are
212 connected to the data acquisition system. Temperature variations in the soil surrounding the

energy foundations are monitored using a series of ten Geokon model 3810 thermistor strings that each have six thermistors spaced equally over the same length as the foundation, installed in boreholes that were then backfilled with CETCO high thermal conductivity grout at the locations shown in Figure 1(a). The temperatures around Foundations 3 and 4 are monitored using four thermistor strings each; with additional thermistor strings located beneath the floor slab and outside the building footprint.

3.5 Ambient Ground Temperatures and Construction Strains

Seasonal temperature vs. depth in Foundation 4 was recorded at various times over the course of a year [Fig. 2(a)], as were the axial strains [Fig. 2(b)]. The depths in this figure (and other figures) are measured from the bottom of the grade beam, which is 0.91 m below the ground surface. Ground temperatures fluctuate between 5 °C and 16 °C near the surface then becomes relatively stable at a temperature of 9 °C at depths below 4 m. The axial strains measured in July 2012 reflect the impact of concrete curing, with some tensile strains observed near the head of the foundation. Construction of the floor slab, walls, and roof occurred in Fall 2012, reflected in the increase in axial strain at the head of the foundation. The difference in the strain profiles between February 2013 and July 2012 was assumed to be equal to the mechanical strain in the foundation due the majority of the building load. The strain decreases with depth as expected, with a maximum strain corresponding to an axial load of 833 kN. Similar behavior was noted from the temperatures and strains measured in Foundations 1 and 3.

3.6 Testing Scheme

A series of thermal response tests were performed on individual and groups of foundations after the building was constructed. Specifically, an 11 kW thermal response test unit was used to circulate and heat a 20% propylene glycol-water mixture through the foundations. The TRT unit is comprised of four heaters, two rated at 2.5 kW and two at 3 kW. A combination of heaters may be activated to achieve a nominal heat input to the heat exchange fluid ranging from 2.5 kW to 11 kW. Fluid properties of the glycol mixture are shown in Table 4. The heated fluid passed into the supply header, circulated through the foundations, and then passed out of return header back to the test unit. The flow rate of each foundation was measured at one instance during the test on each foundation from the pressure/temperature ports (P/T ports) using a differential pressure meter at a fluid temperature of 30 °C. The differential pressure was then used to compute the flow. During the test, the inlet and outlet temperatures of the heat exchanger fluid for each foundation were continuously monitored using pipe plug thermistors installed within ports on the manifold.

A series of seven test stages were performed to investigate the thermal response of various components of the energy foundation system at USAFA, as summarized in Table 5. In each stage, a nominal heat input was selected to avoid heating any foundation component too rapidly. Stage 1 involved heating Foundations 1-4 simultaneously. Since each of these foundations has an

250 identical loop configuration within the foundation itself, the effects of the horizontal length of
251 tubing required to connect each foundation to the manifold (called 'run-out length') was
252 documented (Murphy et al. 2014). Stage 1 operated for 498 hours with the intent of allowing
253 sufficient time to increase the temperature of the soil surrounding the foundations and to observe
254 the temperature rise in the boreholes 3-10. Stages 2-4 were conducted on Foundations 6-8
255 individually with a nominal heat input to the fluid of 5 kW and duration of approximately one
256 week for each stage. Stages 5-7 were conducted on Foundation 5, which has 3 individual loops
257 that can be turned on and off at the manifold. Stage 5 operated on only Loop 5A. During stage 6,
258 Loop 5B of was activated while continuing to pass fluid through Loop 5A. In stage 7, all 3 loops
259 in Foundation 5 were switched open so that flow was permitted to pass through all three loops.
260 Stages 5-7 utilized a 2.5 kW heater in the thermal response test unit. The input heat flux was
261 calculated using Eq. 4 for each heat exchanger loop during each stage.

262 **4 Thermal Response Test Results**

263   The fluid temperatures vs. elapsed time are shown in Figure 3. The differences in fluid
264 temperatures, ΔT, are also plotted on the right vertical axis for each foundation. In all cases, a
265 relatively rapid rise in temperature was observed in the first 25 hours. At one segment during
266 stage 1, the data acquisition system malfunctioned and is represented by a gap in the data [Figs.
267 3(a) to 3(d)]. A constant ΔT value reflects uniform heat input energy into the system, and these
268 conditions prevailed after about 100 hours of testing in each stage. Note that the differential
269 temperature is greater for longer horizontal run-out lengths, indicating that heat exchange occurs
270 in the grade beam and can have an impact on heat exchange performance.

271   The temperatures of the three instrumented foundations at different depths are shown in
272 Figures 4(a), 4(b), and 4(c). The thermistor at the bottom of each of the foundations showed a
273 substantially lower increase in temperature than in the rest of the foundation. This may be due to
274 denser rock at the toe of the foundation, potential rises in the water table at the time of testing, or
275 due to the geometry of how the heat exchangers were routed to the U-connector at the base of the
276 foundation. After approximately 498 hours of heating, fluid circulation in Foundations 1-4 was
277 stopped and the temperatures in the foundation were monitored during the cooling process. The
278 deeper portions of the foundations cooled more rapidly, as they were not influenced by the warm
279 ambient air temperature at the ground surface. The foundations returned to their original
280 temperatures after approximately 700-1000 hours after the end of heating. Fluctuations in the
281 uppermost thermistors during cooling reflect the impact of the seasonal ground temperature
282 fluctuations.

283   Foundation heating led to an increase in ground temperatures measured by the thermistor
284 strings. The temperatures measured in Borehole 1, located at a distance of 4.6 meters outside of
285 the building footprint, are shown in Figure 5(a). The temperature fluctuations occur only near the
286 surface and appear to be due to hot weather. The temperatures measured in Borehole 2, located
287 under the building slab in the center of Foundations 1-4, are shown in Figure 5(b). Although

288 some changes in temperature near the top of the borehole appear to correspond with the increase
289 in surface temperature during the summer, the temperature of the subsurface at the bottom of the
290 borehole experienced an increase in temperature by about 2°C below a depth of 8m likely due to
291 the heating of the subsurface due the operation of Foundations 1-4. After stage 1 ended, the
292 borehole temperature slightly decreased and remained nearly unchanged from 8/15/13 to 9/4/13.

293   The temperatures measured in Boreholes 3 through 6, which are located at different radial
294 distances from Foundation 4, are shown in Figure 6. The temperatures at 1.2 m from the center
295 of Foundation 4 [Figs. 6(a) and 6(b)] increase more rapidly than those located at 2.4 m from the
296 center of the foundation [Figs 6(c) and 6(d)]. The temperatures under the building slab, were
297 affected less by changes in the surface temperature than those that were not under the building
298 slab. This suggests that the floor slab acts as an insulator. This effect may be enhanced after the
299 heating system in the building is used to maintain a constant temperature within the building
300 envelope.

301 **5 Evaluation of Thermo-mechanical Behavior**

302   To evaluate the thermo-mechanical response of the energy foundations, the resonant
303 frequency values, f, from the VWSGs during the heating test were first converted into axial strain
304 ε, as follows:
305

$$\varepsilon = -Gf^2 \qquad \textbf{(5)}$$

306 where G is the gage factor equal to 3.304×10^{-3} and the units of ε are micro-strain. The negative
307 sign follows the geotechnical sign convention where compressive strains are defined as positive.
308 The strain values calculated with Eq. 5 were then converted to thermal strains, as follows:
309

$$\varepsilon_T = [(\varepsilon_i - \varepsilon_0)B + \alpha_s \Delta T] \qquad \textbf{(6)}$$

310
311 where B is the batch calibration factor of 0.975, ε_i is the measured axial strain at time i, ε_0 is the
312 initial value of axial strain at the end of building construction (i.e., ambient temperature), ΔT is
313 the change in temperature between the initial reading and the value at time i, and α_s is the
314 coefficient of thermal expansion of the steel wire of -12.2 $\mu\varepsilon/°C$. This equation accounts for the
315 elongation of the steel wire in the gage during heating.

316   The thermal axial strains calculated using Eq. 6 are shown in Figures 7(a), 7(b), and 7(c). As
317 the temperature increases in the foundations, the thermal axial strains become more negative
318 indicating expansion. The fluctuations in thermal axial strain after heating was stopped correlate
319 well with the observed changes in foundation temperature due to the changes in surface
320 temperature. The strain gauges near the top of each instrumented foundation display the greatest
321 variation, as this is the depth range that is subjected to the greatest change in temperature.

322   Instances in time corresponding to average changes in foundation temperature of 6 °C during
323   heating and cooling were selected to generate thermo-mechanical profiles for each foundation.
324   The profiles of foundation temperature in Figure 8 show that the temperature is relatively
325   constant in the foundation, except for the base of the foundations, and slight variations in the
326   shape of the temperature profile with time are observed in the top of the foundation due to
327   surface temperature effects. The corresponding changes in thermal axial strain are shown in
328   Figure 9. The shapes of the thermal axial strain profiles are relatively consistent for each
329   foundation. A large thermal axial strain at the toe of each foundation was observed even through
330   the change in temperature was not significant. Although this could be due to issues with the
331   temperature measured by the thermistors at these depths, it could also reflect the possibility that
332   the toe of the foundations may be relatively soft. This would be the case if the loose sandstone
333   cuttings were not thoroughly removed from the bottom of the holes during construction. The
334   distributions in thermal axial strain in Figure 9 reflects that soil-structure interaction due to
335   mobilization of side shear resistance leads to a nonlinear distribution in thermal strain with
336   depth, similar to the observations of Laloui et al. (2006) and Bourne-Webb et al. (2009) during
337   the heating portions of their tests.

338   Profiles of thermal axial stress were calculated using Eq. (2) with a Young's modulus of 30
339   GPa (Figure 10). If the foundations were completely restrained, the maximum thermal axial
340   stress that could be generated for an increase in temperature of 18 °C is 6.48 MPa. As the strain
341   gage measurements indicate that some strain occurs in the foundations during heating, the
342   thermal axial stresses in the foundations are all lower than this value. The thermal axial stress
343   generally increases with depth for each of the foundations, although the stress appears to
344   decrease below a depth of 11 to 12 m in each of the foundations. As the point of maximum
345   thermal axial stress typically coincides with the point of zero axial displacements, it is possible
346   that the null point in the foundations occurs at a depth of 11 to 12 m below the grade beam. The
347   thermal axial stresses in Foundation 3 were observed to be nearly 1 MPa lower than in the other
348   two foundations. This could be attributed to the lower amount of restraint provided by the corner
349   of the building compared to the center of the grade beam. Further, Foundations 5 and 8 were not
350   heated, so they may provide greater constraint to Foundations 1 and 4 than to Foundation 3. The
351   thermal axial stresses observed in these three foundations are below 33% of the compressive
352   strength of reinforced concrete (f'$_c$). Even if the foundations were fully restrained (i.e., the case
353   where the measured thermal axial strain is close to zero), the maximum thermal axial stress of
354   6.48 MPa would be less than this limit.

355   The mobilized side shear stress due to changes in foundation temperature was calculated
356   from the difference in thermal axial stress values at different heights in the soil layer, as follows:

$$f_{s,mob,j} = \frac{\left(\sigma_{T,j} - \sigma_{T,j-1}\right)D}{4\Delta l} \tag{7}$$

357 where D is the shaft diameter and Δl is the distance between gages. The sign convention for the
358 mobilized side shear stress implies that positive side shear stresses are upward (in the same
359 direction as those mobilized during mechanical loading), while negative side shear stresses are
360 downward (in the opposite direction as those mobilized during mechanical loading). The
361 mobilized side shear stress profiles calculated for the greatest change in temperature of 18 °C for
362 all three foundations are shown in Figure 11. The results indicate that a negative (downward)
363 side shear stress was observed in the upper portion of the foundation, and a positive (upward)
364 side shear stress was observed in the lower portion of the foundation. The point at which the
365 signs of the mobilized side shear stress changes is in the region of the maximum thermal axial
366 stress and corresponds to the position of the null point. The mobilized side shear stress increases
367 with depth as expected, and the absolute value is less than 200 kPa, which is reasonable for a
368 weakly cemented sandstone.

369 Although the actual displacements of the toe and head of the foundations were not measured,
370 the relative thermal axial displacements to the bottom of the foundations could be calculated by
371 integrating the thermal axial strain profiles, as follows:

$$\delta_{T,i} = \delta_{T,i-1} + \frac{1}{2}(\varepsilon_{T,i-1} + \varepsilon_{T,i})\Delta l \qquad (8)$$

372 where $\delta_{T,i}$ is the thermal axial displacement at the midpoint between gages, $\varepsilon_{T,i}$ is the thermal
373 axial strain at the location of gage i. The profiles of thermal axial displacement for the three
374 foundations suggest that Foundation 3 experienced a greater displacement at the head of the
375 foundation than the other two foundations (Figure 12), likely for similar reasons contributing to
376 the lower thermal axial stress in it. Although the relative displacement at the toe is assumed to be
377 zero for the purposes of calculating the thermal axial displacements, this does not assume that the
378 null point is at the toe. For a rigid, end-bearing foundation, it is expected that the null point
379 should be close to the toe as by definition it should not be able to move downward. If this were
380 the case, then the maximum upward movement of the head would range from -1.3 to -1.7 mm
381 during a change in temperature of about 18 to 19 °C. On the other hand, if loose cuttings are
382 present at the toe, it is possible that the null point would move upward. If the null point is
383 assumed to be at a depth of 11 to 12 m, then the point of zero axial displacement can also be
384 assumed to occur at this depth, shifting the profiles of displacement to the left. In this case, the
385 upward displacement at the foundation head would range from -1.0 to -1.4 mm and the
386 downward displacement at the foundation toe would range from 0.2 to 0.3 mm. If the toe does
387 not move, the maximum upward displacements will lead to an angular distortion δ/L_s, where δ is
388 the difference in displacements of two adjacent energy foundations and L_s is the horizontal
389 spacing between the foundations, of less than 1/5000. This value is lower than the limit expected
390 to cause architectural damage in the building (Skempton and MacDonald 1956, Bjerrum 1963).

391 The foundations experienced linear changes in thermal axial strain with changes in
392 temperature [Fig. 13]. During the cooling phase, the strain for each foundation was observed to

393 nearly return to the values that were experienced during the heating portion of the test, further
394 indicating linear elastic behavior of the reinforced concrete. Relatively little hysteresis was
395 observed, indicating that the mobilized side shear resistance during the heating test did not lead
396 to locked-in plastic strains at the interface. The slope of each trend was defined as the mobilized
397 coefficient of thermal expansion, and the profiles of this coefficient with depth are plotted in
398 Figure 13(d). For each foundation, the mobilized coefficient of thermal expansion was less than
399 that of free expansion ($\alpha_c = -12$ µε/°C), indicating that side shear resistance and the end restraint
400 boundary conditions prevented the foundation from expanding as much as it possibly could in
401 free-expansion conditions. The lowest value of the mobilized coefficient of thermal expansion in
402 each of the foundations was observed at a depth of 11 to 12 m, consistent with the location of the
403 maximum thermal axial stress. Foundation 3 exhibited slightly greater mobilized coefficients of
404 thermal expansion likely due to the lower amount of restraint provided by the corner of the
405 building.

406   The ranges in stress in Foundations 1, 3, and 4 are consistent with those observed from the
407 other full-scale foundations reported in the literature (Table 1). The change in thermal axial
408 stress with the change in temperature for Foundations 1, 3, and 4 are shown along with published
409 data from the literature in Figure 14. The depth corresponding to the greatest increase of thermal
410 stress within each foundation was used to define the maximum rates of axial stress during
411 heating. The depths shown correspond to the null point of each foundation and show the greatest
412 thermal axial stress rate. Rates of $\sigma_t = 210\Delta T$ to $260\Delta T$ were determined from the results in this
413 study, which are slightly higher than values from Laloui et al. (2006) and Bourne-Webb et al.
414 (2009), but are consistent with those calculated from the results of McCartney and Murphy
415 (2012). This may be due to the greater coefficient of thermal expansion of the reinforced
416 concrete used in this study (-12 µε/°C), which is slightly higher than the value of -9.5 µε/°C used
417 in the studies of Laloui et al. (2006) and Bourne-Webb et al. (2009).

418 **6 Evaluation of Thermal Behavior**

419   The details of each heating stage and results from the thermal response tests are summarized
420 in Table 6. The measured heat input for each heat exchanger configuration was normalized over
421 the effective length of the energy foundation system element to define the heat flux per unit
422 meter of heat exchanger Q/L. The effective length, L, is defined as the distance from the
423 manifold to the tip of the foundation. The effective length includes the horizontal run-out length
424 of tubing cast in the grade beam in addition to the 15.2 m length of each foundation. The heat
425 exchange rate is used in this study to assess the relative heat exchange behavior of each
426 foundation because of the geometry of the horizontal connection between the energy foundations
427 and the manifold, which does not satisfy the assumptions of the available analytical methods.
428 The values of Q/L range from 24.4 to 108.5 W/m, which are within the range reported by
429 Bourne-Webb (2013). The value of Q/L was found to be highly dependent on the effective length
430 and nominal heat input, with a decrease in Q/L with increasing effective length. The response is

431   similar to the decrease in heat flux for increasing length to diameter ratios observed by Bourne-
432   Webb (2013).

433   As the horizontal run-out length is increased, the heat exchange rate is observed to decrease
434   as some heat loss or gain occurs in the grade beam (Murphy et al. 2014). The effect of the
435   horizontal run-out length can be assessed by evaluating the Q/L results from Foundations 1
436   through 4, as shown in Figure 15. These foundations have different horizontal run-out lengths,
437   but have the same heat exchanger configuration and were tested together in the same test. A
438   linear relationship was used to estimate the corrected value of Q/L representing the response of a
439   foundation without the effect of horizontal run-out length, as follows:

$$(Q/L)_{corrected} = Q/L - m_{HR} \times H_{RO} \qquad \textbf{(9)}$$

440   where m_{HR} is the run-out length correction factor in (W/m)/m, and H_{RO} is the horizontal run-out
441   length in meters. A value of m_{HR} of -1.16 (W/m)/m was obtained from the slope of the line in
442   Figure 15. The corrected values of Q/L are reported in Table 6. After the correction is applied,
443   values of Q/L for Foundations 1 through 4 ranged from 97.9 to 109.4 W/m. The small
444   differences after correction may be due to the slight difference in flow rate through each of the
445   foundations. The correction approach was applied to the other foundations at the site to eliminate
446   the impact of horizontal run-out length to evaluate the thermal properties of the foundation-soil
447   system alone. The results in Table 6 indicate that Foundation 7 had the highest value of Q/L of
448   132.2 W/m; and it had the longest continuous length of heat exchanger within the foundation.
449   However, Foundations 7 and 8 both have similar high values of Q/L of 120 and 126.9 W/m even
450   though they only have one continuous heat exchanger. It is possible that these tests were not
451   performed for a long-enough duration so that the effect of the heat capacity of the concrete could
452   be overcome (Loveridge and Powrie 2012). The Q/L for Foundation 5 when only loop 5A was
453   included was lower, but this could have been due to the much higher flow rate used in this test.
454   The flow rate decreased when the valves for loops 5B and 5C were opened as flow was
455   distributed amongst the three loops.

456   The thermal conductivity of the subsurface surrounding the foundations could be assessed
457   using the temperatures of the subsurface measured using the thermistor strings in the boreholes.
458   The temperatures of Foundation 4 and the surrounding subsurface were plotted at different
459   instances in time, as shown in Figure 16(a). The vertical line in this figure denotes the outside
460   limit of the building slab, and the distances are measured from the center of the foundation. As
461   expected, as Foundation 4 heats up, the temperature of the soil also increases. The thermal
462   conductivity as a function of time at a depth of 7.3 m was calculated using the temperatures from
463   Boreholes 4 and 5 using Eq. 3, as shown in Figure 16(b). For greater times, the temperature
464   gradient, dT/dr, between the foundation and adjacent boreholes became steadier, which produced
465   thermal conductivity values that were constant between 400 and 500 hours. Thermal
466   conductivity of the soil near the end of heating in stage 1 was calculated to be 2.0 and 2.3 W/mK
467   for heat flow through the subsurface in the directions of Boreholes 4 and 5, respectively. These

468 values of thermal conductivity are consistent with the corrected system thermal conductivity
469 values reported by Murphy et al. (2014) using the line source method to analyze the heating
470 response data reported for stage 1, even though the details of the foundation system do not
471 satisfy the assumptions of this analysis.

7 Conclusions

473 A series of thermal response tests were carried out on eight full-scale energy foundations
474 with various heat exchanger configurations after construction in a new building. Three of eight
475 energy foundations were instrumented with embedded strain gauges and thermistors to capture
476 the thermo-mechanical behavior during heating, while the inlet and outlet fluid temperatures
477 were monitored for each of the foundations to capture their thermal response. Relevant
478 conclusions related to the thermo-mechanical behavior of the energy foundations are as follows:

479 • During heating over a change in temperature of 18 °C, Foundations 1, 3, and 4 experienced a
480   relatively uniform change in temperature with depth.
481 • The increase in temperature led to expansive thermal axial strains in each foundation that
482   were smaller than the estimated free expansion strain. The maximum strains in each
483   foundation occurred near the top and bottom.
484 • The location of the maximum compressive thermal axial stress, which ranged from 4.0 to
485   5.1 MPa, was located between a depth of 11 and 12 m (at a normalized depth of 0.72 to
486   0.78). The thermal axial strains were used to calculate the thermal axial stresses induced in
487   each foundation during heating.
488 • The relative displacement between the head and toe of each instrumented foundation was
489   found to increase nonlinearly upwards. If the toe of the foundation was assumed not to move,
490   the upward displacement of the head of the foundation was estimated to range from -1.3
491   to -1.7 mm for the maximum increase in temperature. However, if the toe of the foundation
492   was assumed to move downward (which would be the case if the hole was not adequately
493   cleaned) and the null point was co-located with the depth of the maximum thermal axial
494   stress, the upward displacement of the head of the foundation was estimated to range
495   from -1.0 to -1.4 mm. In either case, the thermal axial movements are not sufficient to induce
496   structural or aesthetic damage to the building.
497 • The end restraint boundary conditions were found to play an important role in the thermal
498   axial stress and displacement profiles in the energy foundations. Foundation 3 was located at
499   the corner of the building and had the lowest end restraint at the top compared to Foundations
500   1 and 4 which are located beneath the middle of the grade beam, especially considering the
501   fact that Foundations 1 and 4 were also expanding during the same test. The lower head
502   stiffness was found to lead to a lower thermal axial stress in Foundation 3, along with a
503   slightly greater displacement.
504 • The thermal axial strains, stresses, and displacements during cooling were similar to those
505   during heating, indicating linear thermo-elastic behavior. Little hysteresis was observed,

which indicates that permanent thermo-plastic deformations did not occur at the foundation-subsurface interface.

The results from the temperature measured for various system components in each heating stage were analyzed to determine system thermal behavior. Relevant conclusions related to the thermal behavior of the energy foundations are as follows:

- The heat flux ranged from 64.5 to 108.5 W/m for the foundations considering the role of the horizontal run-out length of tubing connecting the foundations to the manifold, although lower values of 34.5 W/m were measured when performing staged heating tests on Foundation 5.
- Heat exchange through the horizontal portion of the loop contributes to the efficiency of heat exchange and may play an important role in the design of the plumbing of energy foundations. After application of a correction factor to consider the effects of the horizontal run-out length, the heat flux ranged from 97.9 to 138.2 W/m, and it was possible to consider the relative impacts of different heat exchange configurations. The foundations with a single heat exchanger loop had relatively high values of heat flux per meter, nearly as high as that of a foundation with 3 continuous heat exchangers. This may be due to the large thermal mass that the single heat exchanger must overcome, leading to a higher Q/L than expected in a long-term test.
- The building slab was observed to lead to an insulating effect that led to more stable temperatures in the subsurface. This issue may become more significant when the temperature of the building is maintained at a constant temperature.
- The temperatures of the subsurface measured using thermistor strings in boreholes surrounding Foundation 4 were used to calculate thermal conductivity of the subsurface. The thermal conductivity at a depth of 7.3 m was observed to range from 2.0 to 2.3 W/mK.

Acknowledgements

References

Adam, D. and Markiewicz, R. (2009). "Energy from earth-coupled structures, foundations, tunnels and sewers." Géotechnique. 59(3), 229-236.

Amatya, B.L., Soga, K., Bourne-Webb, P.J., Amis, T. and Laloui, L. (2012). "Thermo-mechanical behaviour of energy piles." Géotechnique. 62(6), 503–519.

Bjerrum, L. (1963). "Allowable settlement of structures." Proc., European Conf. on Soil Mech. and Found. Engr., Wiesbaden, Germany, Vol. 3, pp. 135- 137.

541 Bourne-Webb, P.J., Amatya, B., Soga, K., Amis, T., Davidson, C. and Payne, P. (2009). "Energy
542   pile test at Lambeth College, London: Geotechnical and thermodynamic aspects of pile
543   response to heat cycles." Géotechnique. 59(3), 237-248.
544 Bourne-Webb, P. (2013). "An overview of observed thermal and thermo-mechanical response of
545   piled energy foundations." European Geothermal Congress. Pisa, Italy. 8 pg.
546 Brandl, H. (2006). "Energy foundations and other thermo-active ground structures."
547   Géotechnique. 56(2), 81-122.
548 Brettmann, T. and Amis, T. (2011). "Thermal conductivity evaluation of a pile group using
549   geothermal energy piles." GeoFrontiers 2012. Dallas, TX. 10 pg.
550 Energy Information Administration (EIA). (2008). Annual Energy Review. Report No.
551   DOE/EIA-0384(2008).
552 Gao, J., Zhang, X., Liu, J., Li, K. and Yang, J. (2008). "Numerical and experimental assessment
553   of thermal performance of vertical energy piles: an application." Applied Energy. 85(10),
554   901-910.
555 Hamada, Y., Saitoh, H., Nakamura, M., Kubota, H. & Ochifuji, K. (2007). "Field performance of
556   an energy pile system for space heating." Energy and Buildings. 39(5), 517–524.
557 Hughes, P.J. (2008). Geothermal (Ground-Source) Heat Pumps: Market Status, Barriers to
558   Adoption, and Actions to Overcome Barriers. Oak Ridge Nat. Lab. Report ORNL-2008/232.
559 Kavanaugh, S., Rafferty, K., and Geshwiler, M. (1997). Ground-Source Heat Pumps – Design of
560   Geothermal Systems for Commercial and Industrial Buildings. ASHRAE. 167 pp.
561 Laloui, L., Nuth, M., and Vulliet, L. (2006). "Experimental and numerical investigations of the
562   behaviour of a heat exchanger pile." International Journal for Numerical and Analytical
563   Methods in Geomechanics 30, 763–781.
564 Laloui, N. and Nuth, M. (2006). "Numerical modeling of some features of heat exchanger pile."
565   Foundation Analysis and Design: Innovative Methods (GSP 153). ASCE. Reston, VA. pp.
566   189-195.
567 Lennon, D.J., Watt, E., and Suckling, T.P. (2009). "Energy piles in Scotland." Proceedings of the
568   5th International Conference on Deep Foundations on Bored and Auger Piles, Frankfurt (Van
569   Impe, W.F. and Van Impe, P.O. (eds)). Taylor and Francis, London, UK.
570 Loveridge, F. and Powrie, W. (2012). "Pile heat exchangers: Thermal behaviour and interactions."
571   Proc. ICE – Geotechnical Engineering. 166(GE2), 178-196.
572 McCartney, J.S. and Murphy, K.D. (2012). "Strain distributions in full-scale energy
573   foundations." DFI Journal. 6(2), 28-36.
574 McCartney, J.S. and Rosenberg, J.E. (2011). "Impact of heat exchange on the axial capacity of
575   thermo-active foundations." GeoFrontiers 2011. Dallas, TX. 10 pg.
576 Mimouni T. and Laloui L. (2013). "Towards a secure basis for the design of geothermal piles."
577   Acta Geotechnica. DOI 10.1007/s11440-013-0245-4. 12 pg.
578 Murphy, K.D. (2013). Evaluation of Thermal and Thermo-mechanical Behavior of Full-scale
579   Energy Foundations. MS Thesis. University of Colorado Boulder.
580 Murphy, K.D., McCartney, J.S., and Henry, K.S. (2014). "Impact of horizontal run-out length on
581   the thermal response of full-scale energy foundations." GeoCongress 2014. Atlanta, GA. 10
582   pg. In press.
583 Ooka, R., Sekine, K., Mutsumi, Y., Yoshiro, S., and SuckHo, H. (2007). "Development of a
584   ground source heat pump system with ground heat exchanger utilizing the cast-in place
585   concrete pile foundations of a building." EcoStock 2007. 8 pp.
586 Ouyang Y., Soga K. and Leung Y.F. (2011). "Numerical back-analysis of energy pile test at

587   Lambeth College, London." Geo-Frontiers 2011, Dallas, TX. pg. 440-449.

588   Sanner, B. (2001). "Shallow geothermal energy." GHC Bulletin. June Issue. pg. 19-25.

589   Sanner, B., Hellstrom, G., Spitler, J., and Gehlin, S.E.A. (2005). "Thermal response test – current
590   status and world-wide application." World Geothermal Congress. Antalya, Turkey.

591   Skempton, A.W. and MacDonald, D.H. (1956), "Allowable settlement of buildings." Proc.
592   Institute of Civil Engineers. London, Part 3, Vol. 5, pp. 727- 768.

593   Stewart, M.A. and McCartney, J.S. (2014). "Centrifuge modeling of energy foundations under
594   cyclic heating and cooling." ASCE Journal of Geotechnical and Geoenvironmental
595   Engineering. 11 pg. In press.

596

597

648 **Table 1. Results of previous studies on thermo-mechanical behavior of energy foundations.**

Case	Laloui et al. (2006)	Bourne-Webb et al. (2009)	McCartney and Murphy (2012); Murphy (2013)
Site stratigraphy	Alluvial soil, sand and gravel, founded in soft sandstone, groundwater table near surface	Granular fill and sand, founded in stiff fissured silty clay, groundwater table at a depth of 3 m	Urban fill, sand and gravel, founded in shale, locations of perched groundwater
Load mechanism at foundation head	Free expansion, building dead load	Load frame	Building dead load
Foundation diameter (m)	0.88	0.56	0.91
Foundation length (m)	25.8	23	14.8 (A), 13.4 (B)
Mechanical load during heating test(s) (kN)	0, 1300	1200	3840 (A), 3640 (B)
Range of ΔT (°C)	+20.9, +13.4	-19.0 to +29.4	-5.0 to +14.0
Depth of minimum thermal axial strain during heating (m)	21.0	17.0	11.6
Minimum/maximum thermal axial stress (MPa)	2.1	-0.8 to 1.9	-1.0 to 5.0
Maximum increase in thermal axial stress with temperature (kPa/°C)	104	192	260
Range in head displacements (negative is upward) (mm)	-4.2, not measured	4.0 to -2.0	0.8 to -1.6

649

650

651   **Table 2. Summary of TRT results from previous studies.**

Case	Hamada et al. (2007)	Ooka et al. (2007)	Gao et al. (2008)	Lennon et al. (2009)	Brettmann and Amis (2011)
Foundation type	26×D.P.	2×D.S.	1×D.S.	4×D.P.	3×A.C.I.P.
Foundation length (m)	9	20	25	12-17	18.3
Foundation diameter (mm)	300 (square)	1500	600	244 (round), 270 (square)	300-450
# Heat exchanger loops	1,2, Indirect/ Direct Pipe	8	1-3	1	2
TRT analysis method	N/A	N/A	Num. Method	Line Source	Line Source
Thermal conductivity (W/mK)	N/A	N/A	5.8-6.0	2.4-2.6	2.5-2.6
Heat exchange rate (W/m)	54-69 (ext.)	100-120 (rej.) 44-52 (ext.)	57-108 (rej.)	N/A	73-80 (rej.)

652   ***D.S.: Drilled shaft, A.C.I.P.: Auger cast in place pile, D.P.: Driven Pile**
653   **** Rej.: Heat rejection into foundation, Ext.: Heat extraction from foundation**
654

655 **Table 3: Summary of stratigraphy encountered during subsurface exploration at USAFA.**

Layer	Depth to bottom of stratum (m)	Material encountered	Gravimetric water content (%)	Dry unit weight (kN/m^3)	SPT N-Value (blows/300 mm)	Thermal Conductivity (W/mK)
1	1	Sandy fill w/ silt, gravel	5	18.4	70	1.118
2	2	Dense sands, silt, gravel	7	19.2	85	0.785
3	12+	Sandstone	N/A	N/A	50/25.4 mm	1.233

656

657 **Table 4. Heat exchange fluid properties.**

Water to propylene glycol ratio	Molar heat capacity (J/molK)	Molecular weight (g/mol)	Specific heat capacity (J/kgK)	Fluid density (g/ml)
5:1	98	30	3267	1.008

658

659 **Table 5. Summary of thermal response testing stages and heat input details.**

Testing stage	Foundation	Testing dates	Approximate duration (hours)	Nominal heat flux applied (kW)	Measured heat flux Q (kW)
1	1 2 3 4	6/18/13 – 7/9/13	498	11.0	3.133 2.696 2.180 2.081
2	6	7/11/13- 7/18/13	175	5.0	4.534
3	7	7/18/13- 7/25/13	167	5.0	4.431
4	8	7/25/13- 8/1/13	165	5.0	4.075
5	5A	8/1/13- 8/5/13	119	2.5	2.285
6	5A 5B	8/5/13- 8/28/13	530	2.5	1.164 1.150
7	5A 5B 5C	8/28/13- 9/4/13	163	2.5	0.797 0.803 1.201

660

661

662 **Table 6: Summary of results from thermal response testing for each stage (Note: all**
663 **foundations have a length of 15.2 m).**

Testing stage	Foundation	Heat exchanger configuration	Effective length, L (m)	Flow rate (ml/s)	Average ΔT_{fluid} (°C)	Measured heat flux, Q (W)	Q/L (W/m)	Corrected Q/L (W/m)
1	1	2 loops	42.6	108	8.8	3133	73.5	105.2
	2		33.5	119	6.9	2696	80.5	101.6
	3		21.3	137	4.8	2180	102.3	109.4
	4		23.6	106	6.0	2081	88.2	97.9
2	6	3 loops	41.8	144	4.8	4534	108.5	139.2
3	7	1 loop	54.0	108	4.5	4431	82.1	126.9
4	8	1 loop in center	63.1	126	3.9	4075	64.6	120.0
5	5A	1 loop	32.7	347	2.0	2285	69.9	90.1
6	5A	1 loop	32.7	226	1.6	1164	35.6	55.8
	5B			226	1.6	1150	35.2	55.4
7	5A	1 loop	32.7	189	1.3	797	24.4	44.6
	5B			189	1.3	803	24.6	44.8
	5C			189	1.9	1201	36.7	56.9

664

665

(a)

(b)

(c)

666
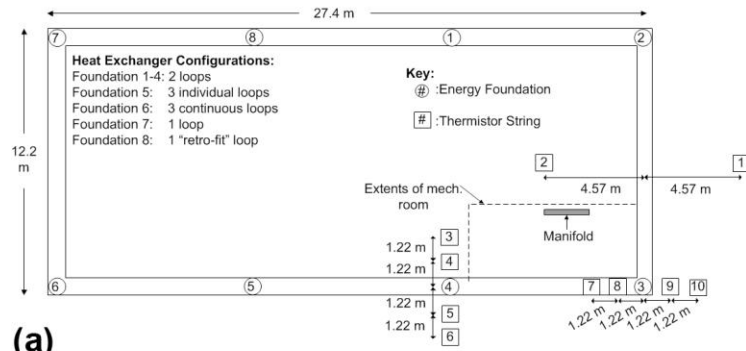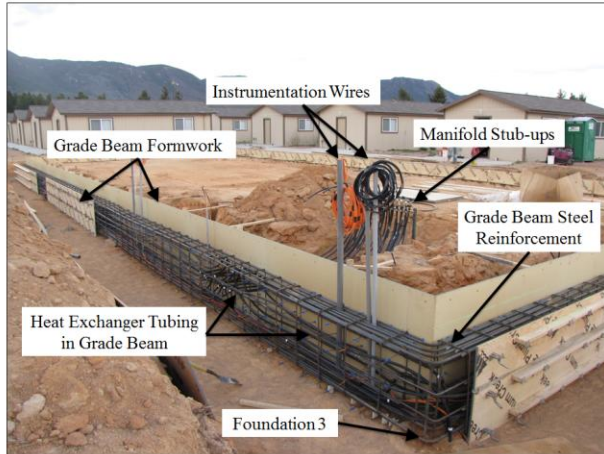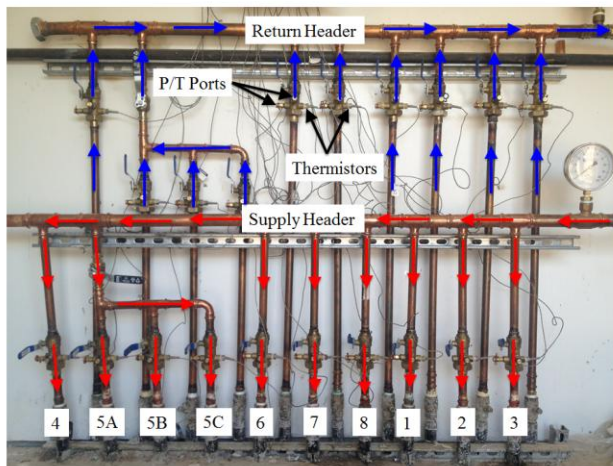
Figure 1. (a) Plan view of the building with the locations of the different energy foundations; (b) Heat exchanger tubing configuration in grade beam prior to concrete placement; (c) Manifold detail prior to installation of insulation.
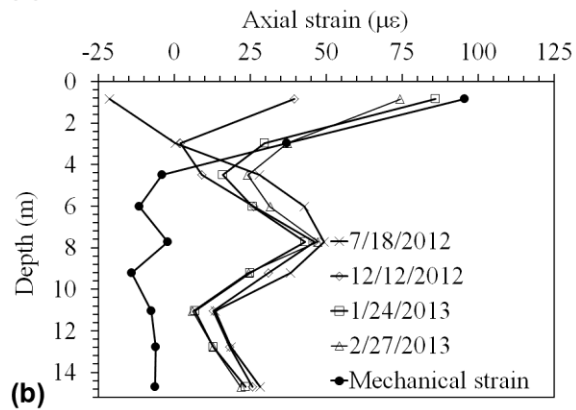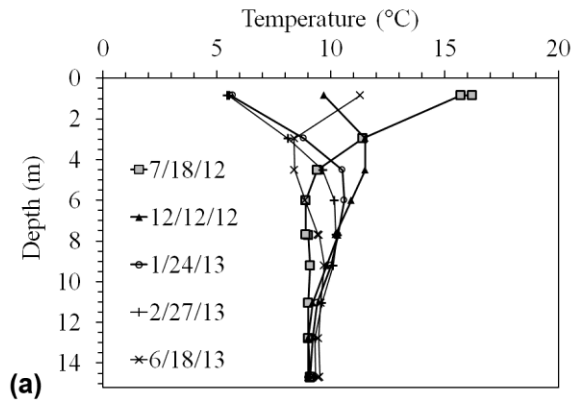
670

671 **Figure 2. Measurements from Foundation 4 during building construction: (a) Profile of**
672 **seasonal temperature variations; (b) Profiles of axial strain during foundation curing**
673 **and building loading, with strains due to mechanical loading.**

674
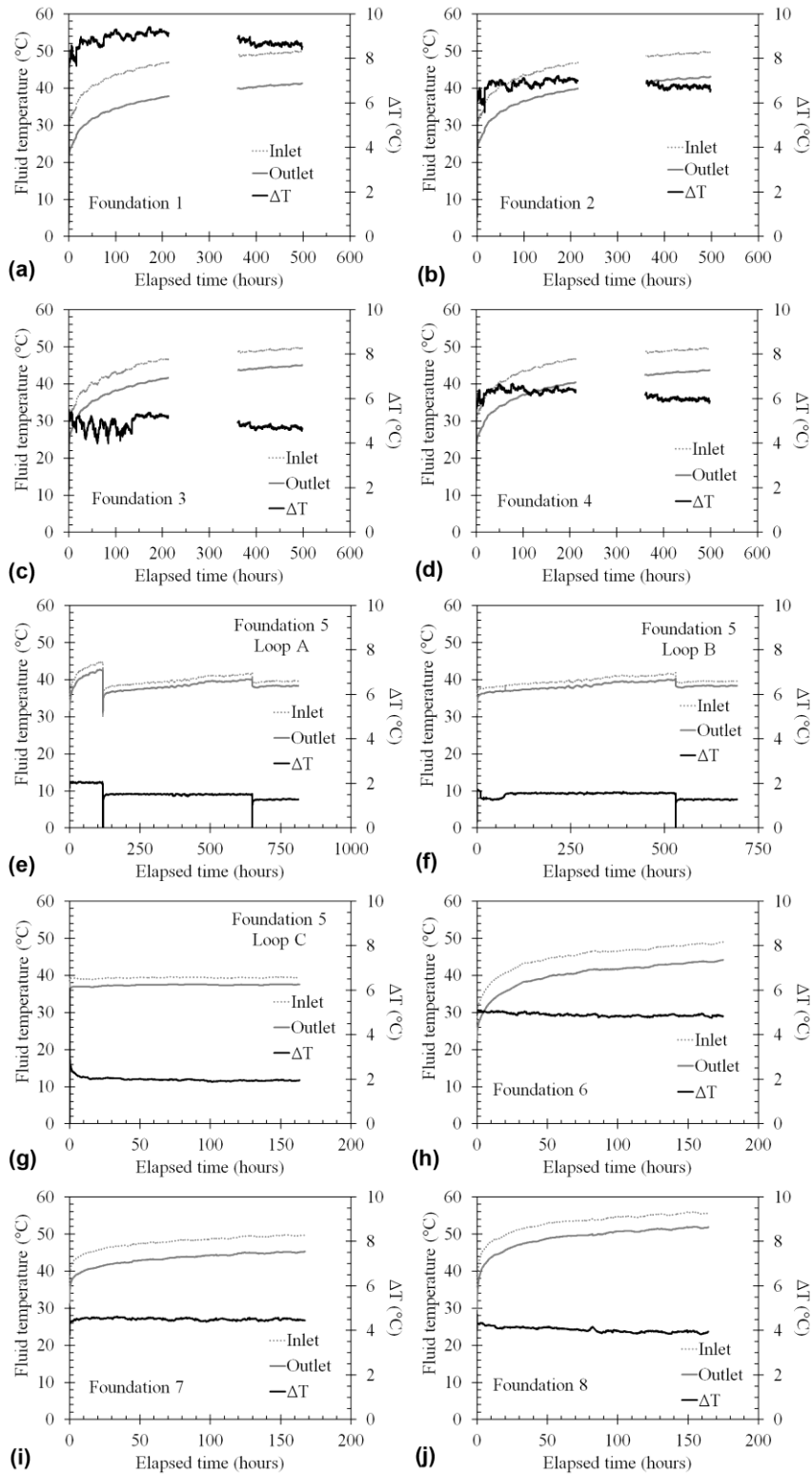
Figure 3. Fluid temperatures during thermal response testing on Foundations: (a) 1 (Stage 1); (b) 2 (Stage 1); (c) 3 (Stage 1); (d) 4 (stage 1); (e) 5, Loop A (stage 5,6,7); (f) 5, Loop B (Stage 6,7); (g) 5, Loop C (Stage 7); (h) 6 (Stage 2); (i) 7 (Stage 3); (j) 8 (Stage 4).

(a)

(b)

(c)

678
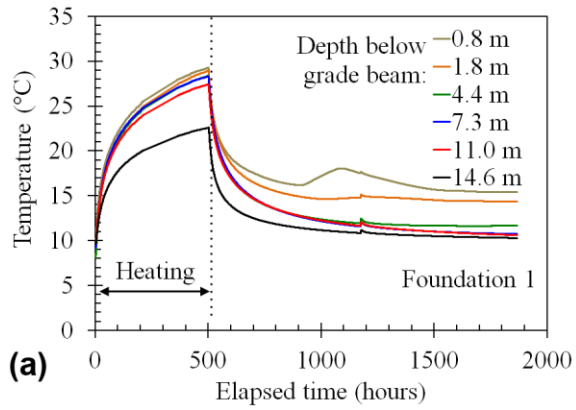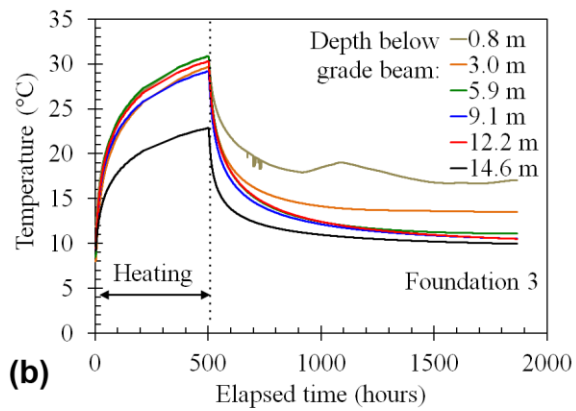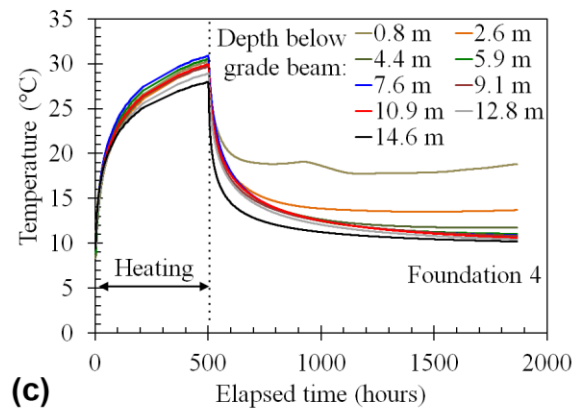
Figure 4. Foundation temperatures during thermal response testing. (a) Foundation 1; (b) Foundation 3; (c) Foundation 4.

681
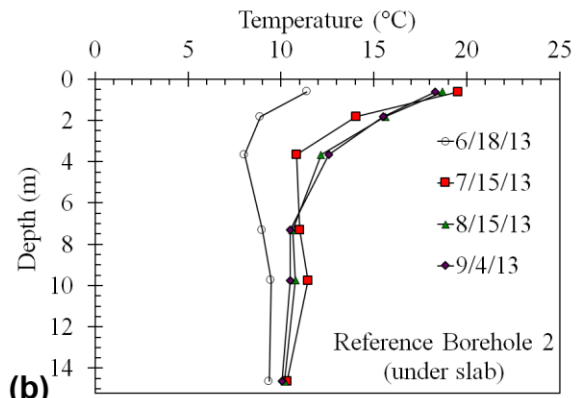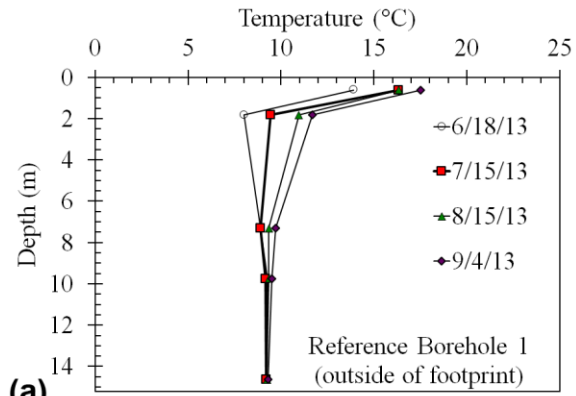
Figure 5. Temperatures of the subsurface during thermal response testing: (a) Reference
Borehole 1; (b) Reference Borehole 2.

684
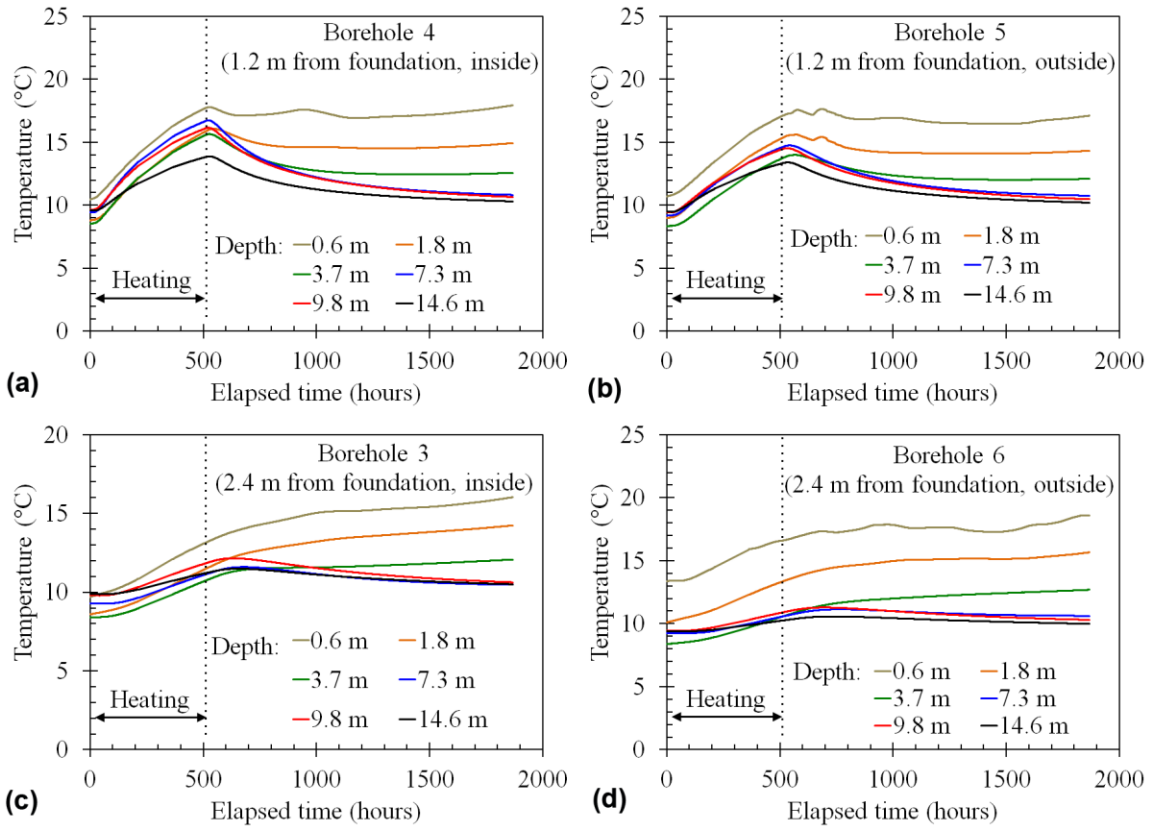
Figure 6. Subsurface temperatures surrounding the foundations during thermal response testing: (a) Borehole 4; (b) Borehole 5; (c) Borehole 3; (d) Borehole 6

(a)

(b)

(c)

687
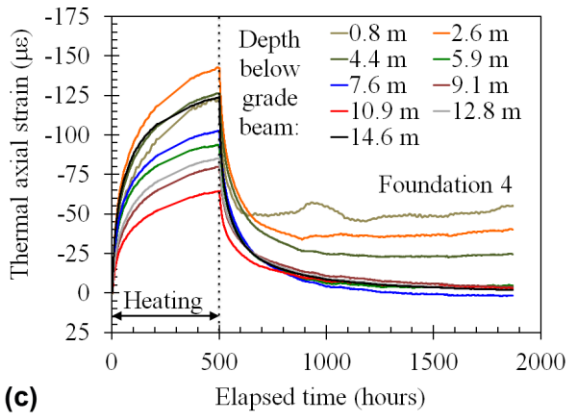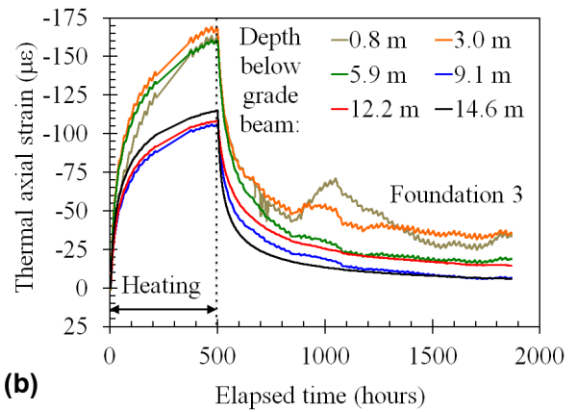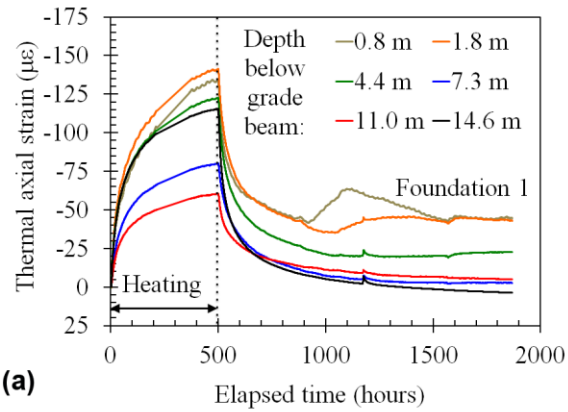
Figure 7: Time series of thermal axial strains during thermal response testing and subsequent cooling: (a) Foundation 1; (b) Foundation 3; (c) Foundation 4

(a)

(b)

(c)

690
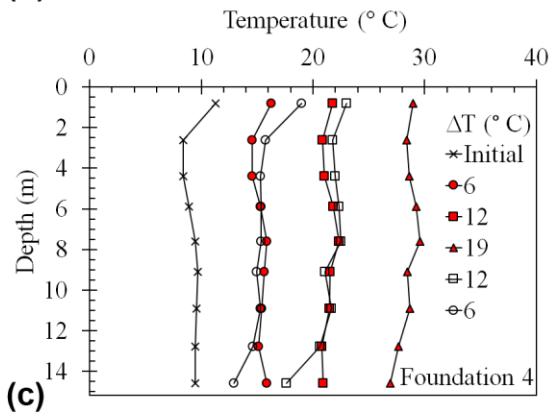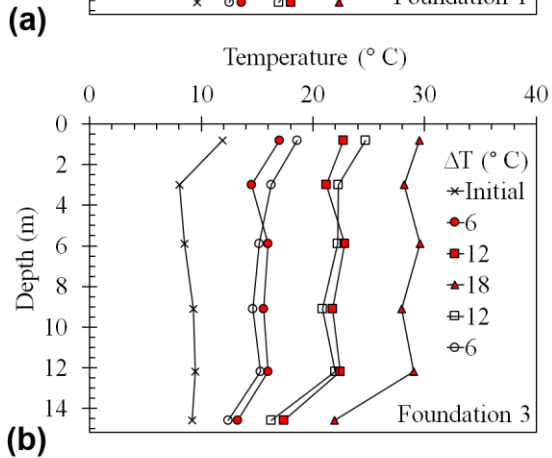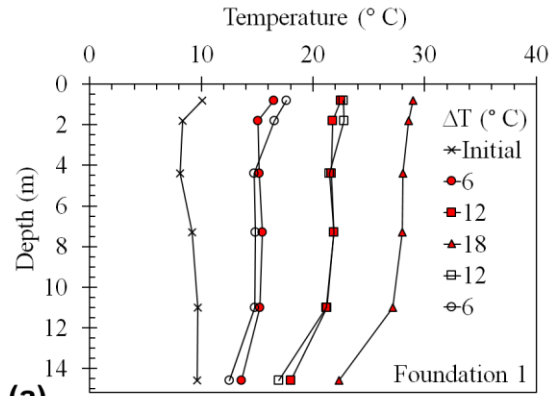
Figure 8: Profiles of temperature for different average changes in foundation temperature during heating (red) and cooling (open): (a) Foundation 1; (b) Foundation 3; (c) Foundation 4
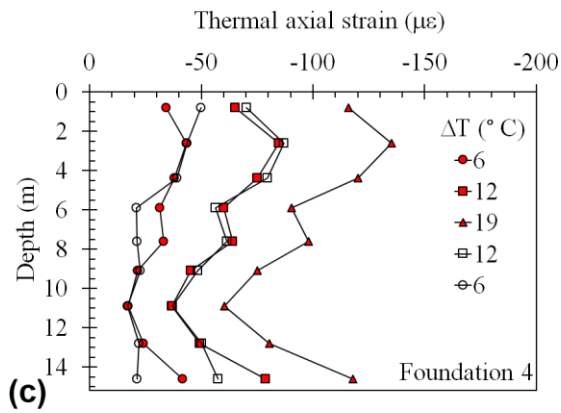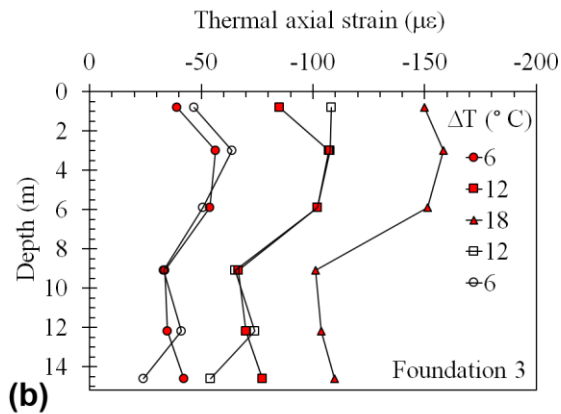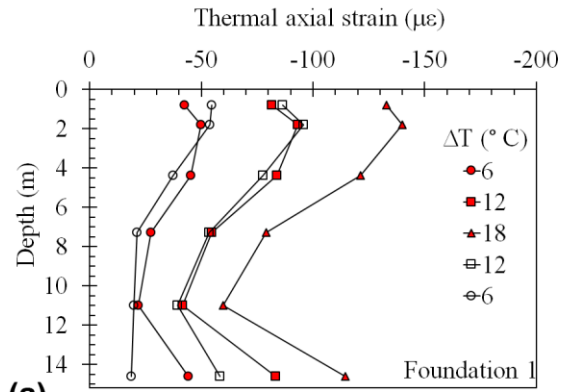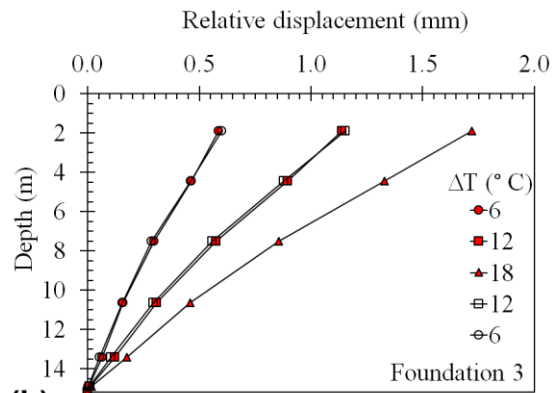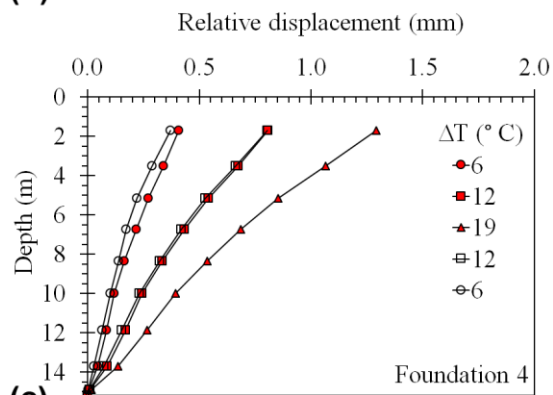
Figure 9: Profiles of thermal axial strain for different average changes in foundation temperature during heating (red) and cooling (open): (a) Foundation 1; (b) Foundation 3; (c) Foundation 4

694

695

696

697

698
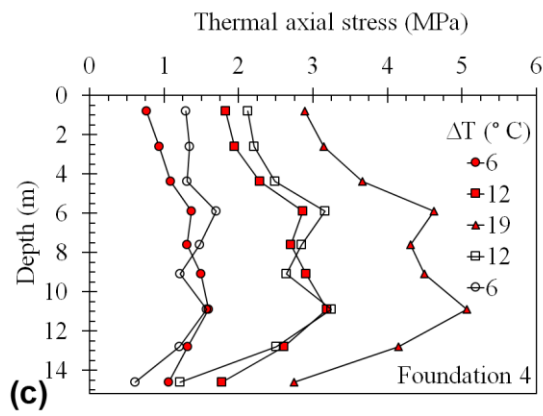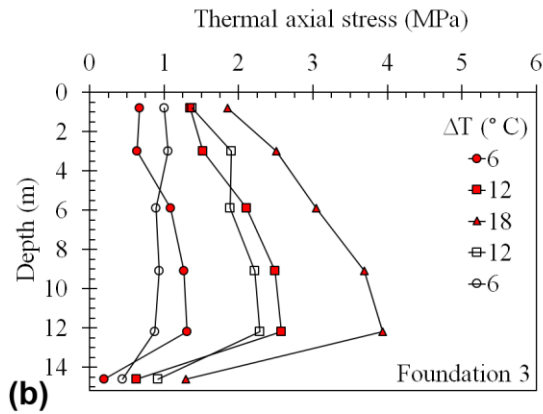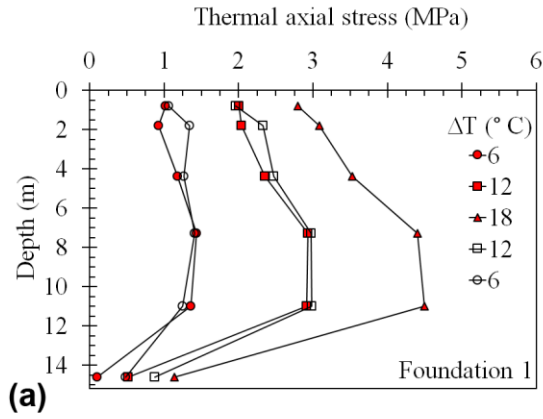
Figure 10: Profiles of thermal axial stress for different average changes in foundation temperature during heating (red) and cooling (open): (a) Foundation 1; (b) Foundation 3; (c) Foundation 4

702
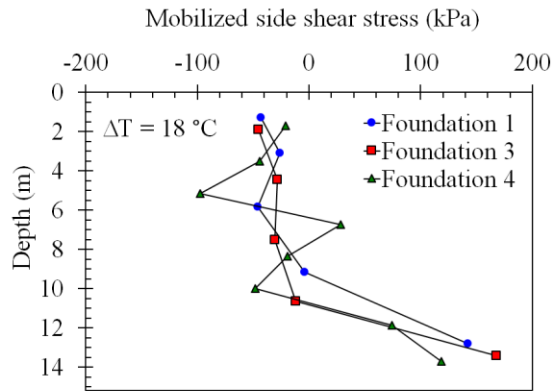
703

704 **Figure 11: Profiles of mobilized side shear for a change in temperature of 18 °C for**
705 **Foundations 1, 3, and 4**

706
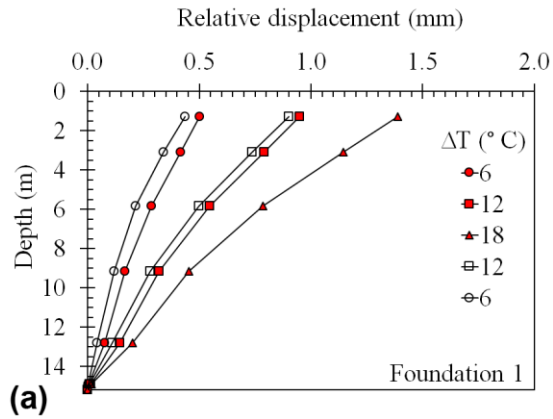
Figure 12: Profiles of thermal axial displacement for different average changes in foundation temperature during heating (red) and cooling (open): (a) Foundation 1; (b) Foundation 3; (c) Foundation 4

710

711
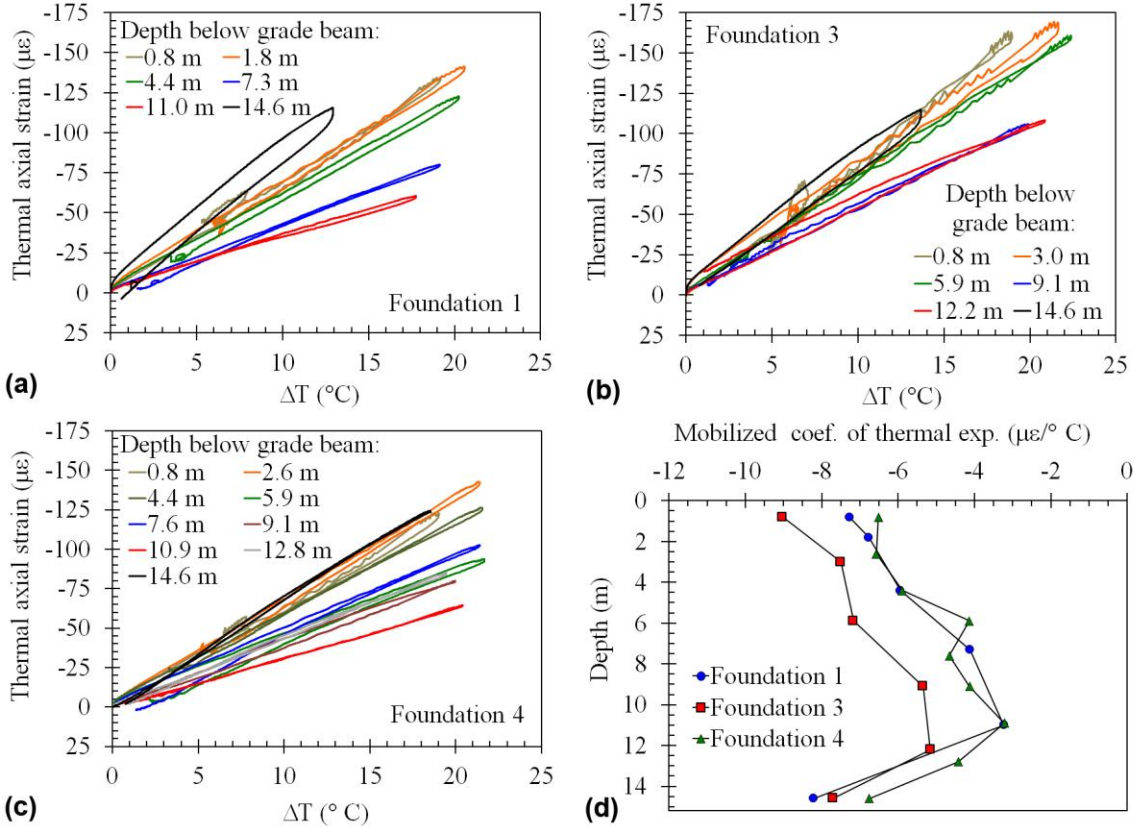
Figure 13. Thermal axial strain with change in foundation temperature at each depth: (a) Foundation 1; (b) Foundation 3; (c) Foundation 4; (d) Mobilized coefficient of thermal expansion with depth for the three instrumented energy foundations.

715
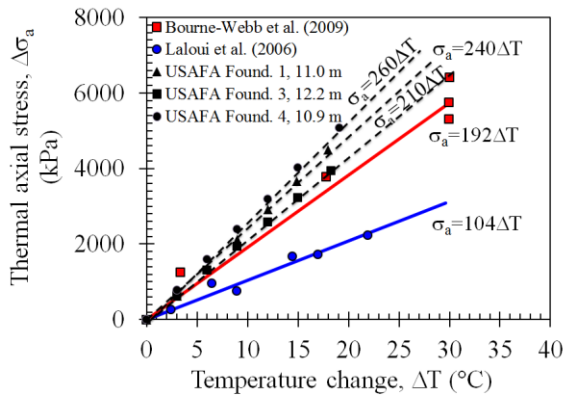
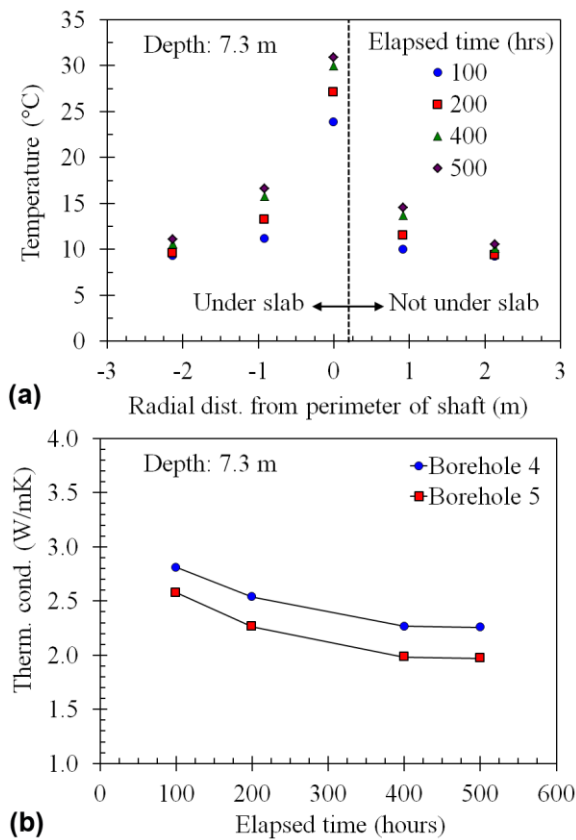**Figure 14. Comparison of the slope of maximum thermal axial stress with change in temperature for the USAFA foundations and those from previous studies.**

718

719

720
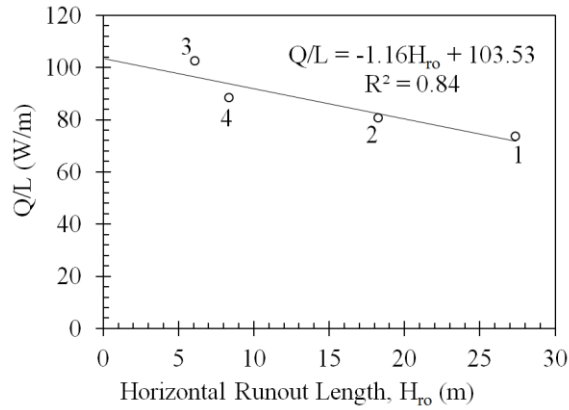
Figure 15. Trends in heat flux per unit meter (Q/L) for Foundations 1 through 4 as a function of horizontal run-out length.

723

Figure 16. (a) Temperatures of Foundation 4 and surrounding soil; (b) Thermal conductivity over the duration of heating from the thermal gradient between the foundation and Boreholes 4 and 5.

727